Vaccinia-Related Kinase 1 is required for early uterine development in *Caenorhabditis elegans*

Agnieszka Dobrzynska and Peter Askjaer*

Andalusian Center for Developmental Biology, CSIC-Junta de Andalucia-Universidad Pablo de Olavide, Carretera de Utrera, km 1, 41013 Seville, Spain.

*Corresponding author: Peter Askjaer (pask@upo.es)

Summary

Protein kinases regulate a multitude of processes by reversible phosphorylation of target molecules. Induction of cell proliferation and differentiation are fundamental to development and rely on tightly controlled kinase activities. Vaccinia-Related Kinases (VRKs) have emerged as a multifunctional family of kinases with essential functions conserved, from nematodes and fruit flies, to humans. VRK substrates include chromatin and transcription factors, whereas deregulation of VRKs is implicated in sterility, cancer and neurological defects. In contrast to previous observations, we describe here that *Caenorhabditis elegans* VRK-1 is expressed in all cell types, including proliferating and post-mitotic cells. Despite the ubiquitous expression pattern, we find that *vrk-1* mutants are particularly impaired in uterine development. Our data show that VRK-1 is required for uterine cell proliferation and differentiation. Moreover, the anchor cell, a specialized uterine cell, fails to fuse with neighboring cells to form the utse syncytium in *vrk-1* mutants, thus providing further insight on the role of VRKs in organogenesis.

Keywords

Anchor cell; Cell fusion; MosSCI; Protein kinase; Uterine development; VRK1

1. Introduction

Elucidation of organogenesis is important in order to understand development of multicellular organisms, and the *Caenorhabditis elegans* egg-laying apparatus serves as an excellent model for studying mechanisms underlying cell fate specification and intercellular signaling pathways (Gupta et al., 2012).

During *C. elegans* development, in late L2 larval stage, two developmentally equivalent cells of the somatic gonad primordium, called Z1.ppp and Z4.aaa, are specified to become either an anchor cell (AC) or a ventral uterine cell (VU; Fig. 1). The AC/VU decision is mediated by the interaction between the receptor LIN-12 (Notch) and its ligand LAG-2, therefore only one of the cells becomes an AC, and the other a VU. The HLH-2 (TCF3/E2A) transcription factor has been shown to directly activate *lag-2* in the presumptive AC and to be post-transcriptionally downregulated in the presumptive VU cell via a negative feedback mechanism (Karp and Greenwald, 2003). Another transcription factor, the *C. elegans* ortholog of the *tailless* nuclear receptor (*nhr-67*), is also implicated in Notch signaling and controls AC specification and development of the uterine π cells (Verghese et al., 2011). When AC fate is determined, six of the eleven ventrally located epidermal Pn.p cells (P3.p – P8.p) are specified as vulva precursor cells (VPCs) by LET-60 (Ras) and Wnt signalling pathways. During the L3 larval stage the AC induces development of the vulva by secreting the epidermal growth factor (EGF-like) ligand LIN-3 to the underlying VPCs so they adopt specific vulval fates (Hill and Sternberg, 1992). The VPCs express the EGF-receptor LET-23 (Aroian et al., 1990), but P6.p, which is in close proximity to the AC, receives the highest level of LIN-3, adopts a 1° cell fate and activates the LIN-12 signaling pathway in the flanking P5.p and P7.p to assume a 2° cell fate. The remaining three VPCs (P3.p, P4.p and P8.p) that receive insufficient inductive or lateral signals adopt a 3° cell fate, divide once and fuse with the syncytial hypodermis (hyp7). After three rounds of divisions, P5.p-P7.p produce 22 vulval cells of seven different types (vulA, vulB1, vulB2, vulC, vulD, vulE, and vulF), which fuse with each other to form seven toroidal rings, connect to the uterus and evert during the last molt to finally form the mature vulva. After induction of the VPCs at the beginning of the L3 larval stage, the AC invades the basement membrane separating the uterine tissue from the underlying developing vulva (Sherwood and Sternberg, 2003). This process is initiated by the formation of F-actin-based invadopodia

enriched for the netrin receptor UNC-40 (Hagedorn et al., 2013). The integrin INA-1/PAT-3 promotes membrane association of UNC-40, phospholipid PI(4,5)P_2, the RacGTPase MIG-2 and F-actin to the invasive cell membrane of the AC (Hagedorn et al., 2009), while secretion of UNC-6 (netrin) from the ventral nerve cord (VNC) guides these components towards the invasive membrane (Ziel et al., 2009). Moreover, cell autonomous signaling of AC, via transcription factor FOS-1A activity, is necessary for basement membrane removal and AC invasion (Sherwood et al., 2005).

The AC also plays a crucial role in uterine morphogenesis. After induction of the central VPCs to adopt vulval fates, the AC signals via LAG-2 and LIN-12 to six of twelve VU descendants to adopt a π cell fate. The π cells divide once and differentiate into two classes; four cells will connect to the dorsal side of the vulva, and eight cells will fuse with the AC during the L4 larval stage and form an H-shaped uterine seam syncytium (utse) (Newman et al., 1996). The utse forms the ventral surface of the uterus. The two long sides of the H shape attach to the lateral seams and hold the uterus in place, while the central part forms a membrane between uterus and vulva, which is broken by the first egg leaving the uterus.

Although the action of several conserved signaling molecules during vulval and uterine morphogenesis is now well established, it is also clear that several pieces are still missing. For instance, LAG-2 is repeatedly used to first specify the AC and then by AC to induce π cells, as well as in signaling between VPCs, indicating the existence of intricate regulatory networks. In contrast, several cues are involved in the correct timing of AC invasion. We have recently described that mutation of *vrk-1* delays anchor cell invasion and abolishes formation of the uterus lumen and utse (Klerkx et al., 2009a).

VRK-1 is a serine-threonine kinase homologous to the human vaccinia-related kinase 1 (VRK1) and belongs to the casein kinase 1 super family. The VRK kinase family is composed of three proteins in vertebrates (VRK1-3), whereas *C. elegans* and *Drosophila* genomes encode a single ortholog (VRK-1 and nucleosomal-histone kinase 1, NHK-1, respectively) (Klerkx et al., 2009b). Human VRK1 phosphorylates several transcription factors including the tumor suppressor p53, c-Jun, ATF2 and CREB (Barcia et al., 2002; Kang et al., 2008; Sevilla et al., 2004a; Sevilla et al., 2004b). Furthermore, VRK1 has a critical role in supporting both chromatin and

nuclear envelope structure by phosphorylating barrier-to autointegration factor (BAF-1 or BANF1) (Gorjanacz et al., 2007; Lancaster et al., 2007; Wiebe and Traktman, 2007). In the absence of VRK1 in *C. elegans* embryos and human cells, BAF-1 remains chromosome-bound upon mitotic entry and defects in chromosome segregation are observed (Gorjanacz et al., 2007; Kim et al., 2013b; Lancaster et al., 2007; Molitor and Traktman, 2014; Wiebe and Traktman, 2007). Interestingly, both inhibition of VRK1 in flies and worms (Cullen et al., 2005; Gorjanacz et al., 2007), as well as overexpression of VRK1 in mammalian cells, lead to hypercondensed chromatin (Kang et al., 2007).

Based on single-copy transgenic strains, we report here that *C. elegans* VRK-1 is more ubiquitously expressed than previously described. We observe that single-copy transgenes rescue *vrk-1* mutant phenotypes more efficiently than multiple-copy transgenes, suggesting that they reflect endogenous levels more accurately. Furthermore, we show that VRK-1 plays a crucial role in uterine development, including π cell specification and proliferation, as well as AC fusion.

2. Materials and Methods

2.1 Nematode strains and transgenesis

C. elegans strains were maintained using standard techniques (Brenner, 1974) and are listed in Supplementary Material Table S1. Single copy transgenic strains were generated by Mos1-mediated single-copy insertion into locus *cxTi10882* of strain EG5003 (Frokjaer-Jensen et al., 2008). Integrated strains were outcrossed to wild type N2 twice. Absence of Mos1 transposon was confirmed by genotyping PCR.

2.2 Plasmids

Plasmids pBN962, pBN961 and pBN1047 with C-terminally located fluorescent tags (GFP, mCherry and Dendra2, respectively; codon-optimized for *C. elegans* and harboring artificial introns) for single-copy expression of VRK-1 contain 870 bp upstream from the *vrk-1* start codon and 1494 bp downstream from the stop codon. Fluorescent tags were inserted into an engineered *BsrG*I site immediately before the stop codon. Plasmid pBN1028 encoding VRK-1 K169E::mCherry was derived from

pBN961 by PCR-stitching to modify *vrk-1* codon number 169 from AAG (K) to GAG (E). Plasmid pBN90 for tissue-specific expression of VRK-1 contains 2194 bp *fos-1c* promoter sequence upstream of the *vrk-1* ORF with C-terminally located mCherry and 301 bp *emr-1* 3'UTR. Detailed cloning information is available upon request.

2.3 Live imaging

For acquisition of single still images, animals were mounted in a 5 μL drop of 10 mM levamisole (tetramisole hydrochloride; Sigma-Aldrich cat. no. L9756, St. Louis, MO, USA) on a 3% agarose pad, covered with a 24 mm × 24 mm coverslip. For long-term imaging, animals were incubated for 30 minutes in 167 μM levamisole, 1.67 mM tricaine (ethyl 3-aminobenzoate methane sulfonate salt; Sigma-Aldrich cat. no. A5040) and then mounted in a 5 μL drop of 167 μM levamisole, 1.67 mM tricaine on a 3% agarose pad, covered with a 24 mm × 24 mm coverslip and sealed with valap (1:1:1 mixture of Vaseline or petroleum jelly, lanolin, and paraffin; melts at 60ºC). Epifluorescence and transmitted light images were acquired using a Nikon A1R confocal microscope through a Plan Apo VC 60x/1.4 objective (Nikon, Tokyo, Japan) or Leica TCS SP2 confocal microscope through a HCX PL APO 63x/1.4 objective. Unless noted otherwise, all comparative images were acquired with identical settings. Quantitative analysis of fluorescence intensity and basal vs. apical polarity ratio after background subtraction were performed using ImageJ and Fiji software. Panels for figures were processed identically for optimal brightness and contrast using Fiji and Adobe Photoshop.

2.4 Rescue experiments

Worms at the L4 stage were placed on NGM plates containing OP50 bacteria and transferred to fresh plates every 8-16 hours. After removal of the adults the number of embryos was scored. Fertile adults and Pvl phenotypes were scored after 72 hours. Experiments were performed at 20˚C.

2.5 Statistical analysis

Data were analyzed by Student's t-test using Microsoft® Excel® except for AC morphology (Fig. 4C) and AC fusion (Fig. 5B) experiments, which were evaluated by Fisher's exact test. Probability values <0.05 were considered significant.

3. Results

3.1 VRK-1 is expressed throughout C. elegans

We initially described postembryonic expression of VRK-1 based on transgenic VRK-1::GFP strains obtained by microparticle bombardment. Observations in these strains suggested that VRK-1 is enriched in neurons in the head and tail, ventral nerve cord (VNC), hypodermal cells and vulva precursor cells (VPCs) (Klerkx et al., 2009a). Microparticle bombardment leads to integration of an unknown copy number of the transgene at a random position in the genome, which can affect the pattern and level of expression (Praitis, 2006). We reported that the VRK-1::GFP transgene introduced by microparticle bombardment reduced the protruding vulva (Pvl) phenotype of *vrk-1* deficient mutants from 75% to 24%. However, adult animals remained sterile, presumably because the transgene was not expressed in the germ line (Klerkx et al., 2009a). To address this, we generated strains using the *Mos1*-mediated Single Copy Insertion (MosSCI) method that leads to integration of a single copy transgene into a defined site and allows expression at endogenous level (Frokjaer-Jensen et al., 2008). We created three constructs for insertion in an intergenic region on chromosome IV, using GFP, mCherry or Dendra2 as fluorescent tags at the carboxyl terminus of VRK-1 followed by the *vrk-1* 3´UTR. Transgenes were expressed under control of the previously described *vrk-1* promoter (Klerkx et al., 2009a). We first compared the single-copy *vrk-1*::GFP fusion gene with the strain obtained by bombardment with a similar *vrk-1*::GFP transgene. The single-copy transgene was expressed at much lower levels and in a more ubiquitous manner (Fig. 2A, Supplementary Material Fig. S1A,B). Importantly, the three transgenes (*vrk-1*::GFP, *vrk-1*::mCherry and *vrk-1*::Dendra2) showed identical expression patterns (Fig. 2A, Supplementary Material Fig. S1A). Nuclear expression was observed, not only in previously reported cells, but also in the anchor cell (AC), uterine tissue and germ line (Fig. 2A). Time-lapse recording of VPC and uterine cell divisions revealed that VRK-1 accumulates at the nuclear envelope at prophase and is associated with

chromosomes in anaphase (Supplementary Material Fig. 2, Video 1) as observed in embryos (Gorjanacz et al., 2007). Multi-copy transgenes are frequently silenced in the *C. elegans* germ line (Kelly et al., 1997), which could explain the lack of VRK-1::GFP expression in the germ line in the strain produced by bombardment. However, even with the single-copy strains we observed considerable variability in germ line expression (ranging from 1/20 to 19/20 animals showing expression), but we note that this has been reported for MosSCI strains (Shirayama et al., 2012).

3.2 Single copy vrk-1 *transgenes rescue mutant phenotypes*

To test if the partial rescue by the bombardment-derived *vrk-1*::GFP transgene was due to the more restricted expression pattern, we analyzed the rescue efficiencies of the single-copy transgenes. We assayed the degree of rescue by counting worms with the Pvl phenotype and brood size (Fig. 2B). When they had reached adulthood, ~100% of wild type hermaphrodites were fertile and did not show the Pvl phenotype. By contrast, 75% of *vrk-1* mutants had a protruding vulva and 100% were sterile. When we introduced single-copy transgenes into the *vrk-1* background, we were able to observe not only a complete rescue of the Pvl phenotype, but also fertility recovery. While 78% and 42% of *vrk-1* mutants of the strains expressing VRK-1::mCherry and VRK-1::Dendra2, respectively, were fertile, almost all *vrk-1* mutants of the strain expressing VRK-1::GFP were sterile (Fig. 2B). The lowest rescue efficiency of the VRK-1::GFP fusion protein is likely to be due to the fact that the frequency of its expression in the germline was also the lowest (two independent lines; data not shown).

We subsequently analyzed whether catalytic activity of VRK-1 is required for correct vulval development and fertility. Substitution of lysine 179 (K179) for glutamic acid (E) in the active site of human VRK1 disrupts its kinase activity (Vega et al., 2004). We introduced the equivalent mutation in VRK-1 (K169E) and generated a single-copy *vrk-1 K169E*::mCherry transgenic strain. The mutated protein was expressed at similar levels and localized in a similar way to wild type VRK-1::mCherry (Fig. 2C). However, all *vrk-1* mutants expressing VRK-1 K169E::mCherry are sterile and 70% have a protruding vulva (Fig. 2B), which supports the argument that VRK-1 functions as an active kinase during development of the reproductive organs in *C. elegans*.

3.3 VRK-1 regulates Anchor Cell morphology

During vulval development the AC becomes polarized and breaches the basement membrane separating vulval and uterine cells. We have previously shown that VRK-1 depletion delays AC invasion in 86% of *vrk-1* mutants and disturbs the basal localization of the actin-binding protein moeABD (Klerkx et al., 2009a). The transcription factor FOS-1A is a key regulator of AC behavior, but FOS-1-independent pathways are also required for proper AC invasion (Sherwood et al., 2005). For instance, HLH-2, which is necessary for specification of AC and VU cells during the early L2 larval stage, is also implicated in the regulation of AC invasion by regulating in a partially FOS-1-independent manner the transcription of protocadherin (*cdh-3*), papilin (*mig-6*) and hemicentin (*him-4*) (Schindler and Sherwood, 2011). Because VRK-1 functions independently from FOS-1 (Klerkx et al., 2009a); (Supplementary Material Fig. S3) we examined whether VRK-1 regulates HLH-2 expression. To minimize genotypic variability we compared *vrk-1* homozygous mutants with heterozygous siblings, which develop as wild type animals. We measured the florescence intensity of GFP::HLH-2 in the AC at the P6.p 1-cell, 2-cell, 4- cell and 6-8-cell stages; however, no differences were observed between control animals and *vrk-1* mutants (Fig. 3A, B). These results suggest that VRK-1 regulates AC invasion independently of the HLH-2 pathway.

In order to decipher whether the *vrk-1* mutation affects markers of AC polarization and invasion other than moeABD, we analyzed the localization of the netrin receptor UNC-40 (DCC) fused to GFP, the phospholipaseC-δ *(*PLCδ^{PH}*)* fused to mCherry, the beta-integrin subunit PAT-3 fused to GFP and finally MIG-2, a member of the Rho family of GTP-binding proteins, fused to GFP. We examined the polarity of the AC by measuring the average fluorescence intensity of the basal (invasive) versus apical (noninvasive) membranes of the AC. In control animals, UNC-40, MIG-2, PLCδ^{PH}, and PAT-3 accumulates at the invasive membrane of the AC (Hagedorn et al., 2009; Ziel et al., 2009). In *vrk-1* mutants the fusion proteins were enriched at the invasive membrane of the AC to a similar degree to that in control animals, except PAT-3, which was slightly hyperpolarized (Fig. 4A, B). Interestingly, we observed that AC morphology was severely affected in *vrk-1* mutants. While the apical side of the AC usually had a rounded dome shape in control animals at the P6.p 4-cell stage, it was

more irregular in *vrk-1* mutants and cell protrusions were observed more frequently (Fig. 4A, C).

3.4 Anchor Cell fails to fuse in C. elegans vrk-1 mutants

The abnormal AC morphology in the absence of VRK-1 combined with the previous observation that the utse is not formed in *vrk-1* mutants (Klerkx et al., 2009a) prompted us to investigate the AC fusion process. To this end, we assayed a *cdh-3::gfp* reporter as marker of AC fusion (Hanna-Rose and Han, 1999; Pettitt et al., 1996). CDH-3 is a member of the cadherin superfamily, which is implicated in cell adhesion, regulation of tissue organization and morphogenesis (Pettitt, 2005). The *cdh-3* reporter expresses soluble GFP in the AC during the L3 larval stage and as the AC fuses with descendants of uterine π cells, GFP spreads from the AC cytoplasm throughout the utse cell (Hanna-Rose and Han, 1999). It is also expressed in VPCs and uterine epithelium closest to the invaginating vulva (Pettitt et al., 1996). As expected, we observed a strong fluorescence signal of *cdh-3*::GFP in the AC during the L3 stage, both in control animals and *vrk-1* mutants (Fig. 5A). However, when the fusion of the AC during L3/L4 molt caused a dilution of the GFP signal in control animals, in most *vrk-1* mutants (17/24) GFP was confined to the area of the AC, suggesting that the AC fails to fuse in *vrk-1* mutants (Fig. 5A, C). A minor fraction of *vrk-1* mutants (5/24) presented an ambiguous phenotype, resulting from abnormal AC morphology and *cdh-3*::GFP expression in the VPCs and, in lower levels, in other uterine cells.

To confirm that the lack of AC fusion is a result of the *vrk-1* mutation, we expressed VRK-1::mCherry specifically in the uterine tissue. As described above, *vrk-1* does not regulate *fos-1* expression, which facilitates using the *fos-1c* promoter that was identified as a uterine intermediate precursor enhancer (Oommen and Newman, 2007). When we expressed low levels of VRK-1::mCherry from a single-copy transgene under control of the *fos-1c* promoter, we rescued the lack of AC fusion in *vrk-1* mutants, as well as formation of the utse and the uterine lumen (Fig. 5B, C, Supplementary Material Fig. S4). These data confirmed that VRK-1 is necessary for fusion between the AC and uterine π cells and that VRK-1 expression in the uterine tissue is sufficient for this process.

3.5 Lack of VRK-1 causes proliferation and differentiation defects in uterine cells

We next sought to determine the onset of uterine defects in *vrk-1* mutants by analyzing the expression of HLH-2 and *tailless* ortholog NHR-67 during earlier developmental stages. The AC, as other uterine cells, is derived from cells of the somatic gonad primordium. In the L2 larval stage NHR-67 is expressed in the four pre-VU cells that become the AC and three VU cells (Verghese et al., 2011). Moreover, during AC/VU decision, HLH-2 is expressed in both Z1.ppp and Z4.aaa precursor cells and as AC/VU decision progresses, its expression is elevated in the presumptive AC to activate *lag-2* transcription (Karp and Greenwald, 2003; Schindler and Sherwood, 2011). We found that all four pre-VU cells expressed NHR-67::GFP in both control animals and *vrk-1* mutants (Fig. 6A) and the ratio of GFP::HLH-2 expression between the presumptive AC and the adjacent VU cell was also normal (Supplementary Material Fig. S5). These observations suggest that initial specification of AC and VU linages is *vrk-1* independent and that defects leading to abnormal AC morphology and behavior occur later in L3 larvae.

We therefore analyzed the expression of EGL-13, a SOX domain transcription factor, fused to GFP. EGL-13 is controlled dually by FOS-1 and LAG-1 and is required for the maintenance of the uterine π cell fate (Oommen and Newman, 2007). In concordance with our previous description of diminished LIN-11 expression, we observed a reduced number of cells expressing EGL-13::GFP upon loss of *vrk-1,* confirming abnormal uterine π cell specification in *vrk-1* mutants (Fig. 6B). In order to decipher whether VRK-1 depletion affects proliferation of the uterine cells, we used HIS-72::GFP and EMR-1::mCherry to mark chromatin and nuclear envelopes, respectively. Affected morphology of the uterine tissue was described at the L4 larval stage (Klerkx et al., 2009a) but earlier stages have not been analyzed. We observed that both the number of uterine nuclei and their morphology were severely affected at early L3 larval stage (Fig. 6C). In control animals, uterine nuclei were surrounded by uniform EMR-1::mCherry signal, whereas they were smaller and with irregular EMR-1::mCherry distribution in *vrk-1* mutants. Later, at the L3/L4 molt, these defects were exacerbated, while neighboring vulva cells had normal morphology, demonstrating that uterine cells are more sensitive to loss of VRK-1 function (Fig. 6C). Similarly, using FOS-1::YFP to specifically visualize uterine cells also clearly indicated that the

number of FOS-1A::YFP expressing nuclei is lower in *vrk-1* mutants (Fig. 6D). Single-copy expression of VRK-1 specifically in the uterine tissue, under control of the *fos-1c* promoter, rescued not only defects in the morphology and number of FOS-1-expressing uterine cells, but also the Pvl phenotype (Fig. 6E, F). We did not observe rescue of the fertility, which agrees with the restricted expression of *vrk-1* in the uterine cells, but not in the germ line, from the *fos-1c* promoter. From these observations we conclude that *vrk-1* is necessary for proper proliferation and differentiation of uterine tissue in a cell autonomous manner.

4. Discussion

4.1 VRK-1 is expressed ubiquitously

In this study we have shown that *vrk-1* is ubiquitously expressed, including all vulva and uterine cells. Fusion between the AC and surrounding π cells to form the utse is inhibited in *vrk-1* mutants, which causes a penetrant Pvl phenotype. The Pvl phenotype is efficiently rescued by fluorescent VRK-1 fusion proteins, but not by a kinase-dead VRK-1 K169E mutant, indicating that vulval development requires VRK-1 kinase activity. Notably, ectopic expression of *vrk-1*, specifically in uterine cells, efficiently rescues vulval and uterine development, suggesting that VRK-1 acts cell autonomously. This is in contrast to our previous conclusion that VRK-1 expression in vulva cells regulates AC behavior in a cell non-autonomous manner (Klerkx et al., 2009a). This conclusion was based on two observations. Firstly, a *vrk-1* RNAi hairpin expressed from the *lin-31* promoter in RNAi spreading-defective animals produced a Pvl and/or Egl phenotype with 20% penetrance. The *lin-31* promoter was chosen based on its activity in VPCs (Tan et al., 1998). However, others have reported a more broad expression pattern of *lin-31* (Reece-Hoyes et al., 2007), suggesting that *vrk-1* could have been knocked down in several cell types. Secondly, microparticle bombardment-derived *vrk-1::gfp* transgenes that were expressed in the VNC and VPCs, but not in the AC and uterine tissue, restored uterine development in *vrk-1* mutants. Microparticle bombardment typically produces higher expression than MosSCI, presumably because the former often introduces several copies of the transgene into the genome (Frokjaer-Jensen et al., 2008). Comparison of *vrk-1* bombardment and MosSCI strains indeed revealed lower, but also more

widespread expression in the latter, including most proliferating and post-mitotic cells. Importantly, whereas the *vrk-1* bombardment strain reduced the Pvl phenotype of *vrk-1* mutants from 75% to 24% (Klerkx et al., 2009a), our new single-copy strains completely suppressed this phenotype. Germ-line expression and fertility was only rescued by the MosSCI strains. We therefore propose that the transgenic *vrk-1* expression pattern reported here more accurately reflects the behavior of endogenous *vrk-1*. Like many other *C. elegans* genes, *vrk-1* is situated in an operon, which makes transgene construction more challenging. Although we expressed *vrk-1* under control of the putative, directly upstream endogenous promoter, it is possible that it does not fully recapitulate the native expression pattern. To address this, we have repeatedly tried to use CRISPR/Cas9, a novel method of genome engineering (Waaijers and Boxem, 2014) to knock-in *mCherry* into the endogenous *vrk-1* locus, however to date we have not succeeded. Moreover, we have raised several antibodies against VRK-1 but none of them has worked satisfactorily in an immunohistological analysis of larval and adult tissues.

Although we favor the possibility that endogenous *vrk-1* is expressed in all uterine cells, including the AC, our earlier conclusion that AC invasion timing, as well as formation of the utse and the uterine lumen, could be rescued by cell non-autonomous overexpression of *vrk-1::gfp*, poses an interesting question: Does VRK-1 act in tissues surrounding the uterus (e.g. the developing vulva, intestine, hypodermis, etc.) to guide uterine development, or is the requirement for cell autonomous expression of *vrk-1* in uterine cells, including the AC, so low that sufficient, but undetectable quantities might be expressed in the *vrk-1* bombardment strain? The data presented here on ectopic *vrk-1* expression from the uterine-specific *fos-1c* promoter, which expressed less VRK-1::mCherry than the *vrk-1* promoter, suggests a cell autonomous role of VRK-1 in uterine cells, although it does not rule out a *vrk-1*-mediated contribution from other tissues. In any case, our results point to the need to be cautious about site-of-action studies, in particular with multi-copy transgenes.

4.2 Control of cell morphology and fusion by VRK-1

The actin-binding protein, moeABD, accumulates abnormally at the apical, noninvasive, membrane of the AC in *vrk-1* mutants, suggesting a role of VRK-1 in

the pathways controlling AC polarization (Klerkx et al., 2009a). However, we did not observe differences in the asymmetric distribution of three other proteins involved in the AC polarization, and PAT-3 was only mildly mis-localized. PAT-3 is a beta subunit of integrin, which regulates F-actin recruitment at the cell membrane (Hagedorn et al., 2009), therefore we expected the apically accumulated moeABD in *vrk-1* mutants to coincide with increased amounts of PAT-3 at the apical AC membrane. However, quantification of PAT-3 polarity suggested a mild hyperpolarization of the basal membrane of the AC in *vrk-1* mutants. Upon depletion of VRK-1, morphology of the uterine cells, including the AC, is affected, whereas the vulva tissue is normal. Rather that having a typical smooth dome-shaped apical side, the AC was frequently characterized by long protrusions in *vrk-1* mutants. The apical accumulation of moeABD in *vrk-1* mutants might therefore reflect abnormal actomyosin cytoskeleton distribution induced by irregular contacts between the AC and other uterine cells rather than AC mis-polarization. Signaling from the AC to uterine cells is required in order for the latter to adopt the π cell fate, however, π cell markers are not correctly expressed in *vrk-1* mutants (Klerkx et al., 2009a) (and this study). Perhaps as a consequence hereof, the AC does not fuse to its neighboring uterine cells and the utse is therefore not formed, ultimately causing protrusion of the vulva. Importantly, as indicated above, expression of *vrk-1* specifically in the uterine cells (including the AC), was sufficient to rescue both AC fusion and the Pvl phenotype.

4.3 VRK-1 and cell cycle control

RNAi against *vrk-1* leads to early embryonic lethality (Gorjanacz et al., 2007), however, homozygous *vrk-1* mutants produced by heterozygous hermaphrodites are viable and do not show any evident defects until the early L3 larval stage, which can be explained by the maternal contribution of mRNA and protein. We show in this study that fates of both AC and VU cells are properly specified during the L2 larval stage in the absence of VRK-1, but the morphology of uterine nuclei is severely affected at the early L3 larval stage, prior to uterine morphogenesis. Moreover, mitotic progression and morphology of germ line nuclei is also disrupted in *vrk-1* mutants (Waters et al., 2010). However, we also note that nuclear appearance of VPCs, which continue to divide after the uterine cell division and morphology defects

described here, is not affected in *vrk-1* mutants (Klerkx et al., 2009a) (and this study). This suggests that VRK-1 might regulate cell proliferation in a cell-type specific manner, involving both nuclear envelope disassembly (Gorjanacz et al., 2007) and cell cycle progression (Waters et al., 2010). The role of VRK-1 in the cell cycle is likely to be evolutionary conserved. For instance, inhibition of VRK1 in human cell cultures causes a block in progression from the G1 to S phase and its expression parallels that of c-*myc* and c-*fos,* which are early response genes (Valbuena et al., 2008). Moreover, VRK1 regulates cell cycle progression by phosphorylation of the cAMP-response element-binding protein and increasing cyclin D1 expression (Kang et al., 2008). These activities of VRK1 are likely to have tissue-specific implications, as reduction of VRK1 expression in mice is linked to gametogenesis defects and infertility (Schober et al., 2011; Wiebe et al., 2010). In concordance with VRK1's role in controlling cell cycle progression and proliferation, several recent studies have identified VRK1 as an attractive target for development of new anti-cancer therapies (Baratta et al., 2015; Kim et al., 2013a; Kim et al., 2014; Riggi et al., 2014; Salzano et al., 2014). We propose that organogenesis in *C. elegans* might serve as a useful tool to evaluate the underlying mechanisms.

Acknowledgements

We are indebted to Cristina Ayuso García for her excellent technical assistance. We wish to thank Antonio Miranda Vizuete for his insightful comments and discussions. We gratefully acknowledge funding from the Spanish Ministry of Economy and Competitiveness (BFU2013-42709P), the Autonomous Government of Andalusia (P08-CVI-3920) and the European Regional Development Fund to P.A. and a postdoctoral contract from the Autonomous Government of Andalusia to A.D.

References

Aroian, R.V., Koga, M., Mendel, J.E., Ohshima, Y., Sternberg, P.W., 1990. The let-23 gene necessary for Caenorhabditis elegans vulval induction encodes a tyrosine kinase of the EGF receptor subfamily. Nature 348, 693-699.

Baratta, M.G., Schinzel, A.C., Zwang, Y., Bandopadhayay, P., Bowman-Colin, C., Kutt, J., Curtis, J., Piao, H., Wong, L.C., Kung, A.L., Beroukhim, R., Bradner, J.E.,

Drapkin, R., Hahn, W.C., Liu, J.F., Livingston, D.M., 2015. An in-tumor genetic screen reveals that the BET bromodomain protein, BRD4, is a potential therapeutic target in ovarian carcinoma. Proc Natl Acad Sci U S A 112, 232-237.

Barcia, R., Lopez-Borges, S., Vega, F.M., Lazo, P.A., 2002. Kinetic properties of p53 phosphorylation by the human vaccinia-related kinase 1. Arch Biochem Biophys 399, 1-5.

Brenner, S., 1974. The genetics of Caenorhabditis elegans. Genetics 77, 71-94.

Cullen, C.F., Brittle, A.L., Ito, T., Ohkura, H., 2005. The conserved kinase NHK-1 is essential for mitotic progression and unifying acentrosomal meiotic spindles in Drosophila melanogaster. J Cell Biol 171, 593-602.

Frokjaer-Jensen, C., Davis, M.W., Hopkins, C.E., Newman, B.J., Thummel, J.M., Olesen, S.P., Grunnet, M., Jorgensen, E.M., 2008. Single-copy insertion of transgenes in Caenorhabditis elegans. Nat Genet 40, 1375-1383.

Gorjanacz, M., Klerkx, E.P., Galy, V., Santarella, R., Lopez-Iglesias, C., Askjaer, P., Mattaj, I.W., 2007. Caenorhabditis elegans BAF-1 and its kinase VRK-1 participate directly in post-mitotic nuclear envelope assembly. EMBO J 26, 132-143.

Gupta, B.P., Hanna-Rose, W., Sternberg, P.W., 2012. Morphogenesis of the vulva and the vulval-uterine connection. WormBook, 1-20.

Hagedorn, E.J., Yashiro, H., Ziel, J.W., Ihara, S., Wang, Z., Sherwood, D.R., 2009. Integrin acts upstream of netrin signaling to regulate formation of the anchor cell's invasive membrane in C. elegans. Dev Cell 17, 187-198.

Hagedorn, E.J., Ziel, J.W., Morrissey, M.A., Linden, L.M., Wang, Z., Chi, Q., Johnson, S.A., Sherwood, D.R., 2013. The netrin receptor DCC focuses invadopodia-driven basement membrane transmigration in vivo. J Cell Biol 201, 903-913.

Hanna-Rose, W., Han, M., 1999. COG-2, a sox domain protein necessary for establishing a functional vulval-uterine connection in Caenorhabditis elegans. Development 126, 169-179.

Hill, R.J., Sternberg, P.W., 1992. The gene lin-3 encodes an inductive signal for vulval development in C. elegans. Nature 358, 470-476.

Kang, T.H., Park, D.Y., Choi, Y.H., Kim, K.J., Yoon, H.S., Kim, K.T., 2007. Mitotic histone H3 phosphorylation by vaccinia-related kinase 1 in mammalian cells. Mol Cell Biol 27, 8533-8546.

Kang, T.H., Park, D.Y., Kim, W., Kim, K.T., 2008. VRK1 phosphorylates CREB and mediates CCND1 expression. J Cell Sci 121, 3035-3041.

Karp, X., Greenwald, I., 2003. Post-transcriptional regulation of the E/Daughterless ortholog HLH-2, negative feedback, and birth order bias during the AC/VU decision in C. elegans. Genes Dev 17, 3100-3111.

Kelly, W.G., Xu, S., Montgomery, M.K., Fire, A., 1997. Distinct requirements for somatic and germline expression of a generally expressed Caernorhabditis elegans gene. Genetics 146, 227-238.

Kim, I.J., Quigley, D., To, M.D., Pham, P., Lin, K., Jo, B., Jen, K.Y., Raz, D., Kim, J., Mao, J.H., Jablons, D., Balmain, A., 2013a. Rewiring of human lung cell lineage and mitotic networks in lung adenocarcinomas. Nature communications 4, 1701.

Kim, W., Lyu, H.N., Kwon, H.S., Kim, Y.S., Lee, K.H., Kim, D.Y., Chakraborty, G., Choi, K.Y., Yoon, H.S., Kim, K.T., 2013b. Obtusilactone B from Machilus Thunbergii targets barrier-to-autointegration factor to treat cancer. Mol Pharmacol 83, 367-376.

Kim, Y.S., Kim, S.H., Shin, J., Harikishore, A., Lim, J.K., Jung, Y., Lyu, H.N., Baek, N.I., Choi, K.Y., Yoon, H.S., Kim, K.T., 2014. Luteolin suppresses cancer cell proliferation by targeting vaccinia-related kinase 1. PLoS One 9, e109655.

Klerkx, E.P., Alarcon, P., Waters, K., Reinke, V., Sternberg, P.W., Askjaer, P., 2009a. Protein kinase VRK-1 regulates cell invasion and EGL-17/FGF signaling in Caenorhabditis elegans. Dev Biol 335, 12-21.

Klerkx, E.P., Lazo, P.A., Askjaer, P., 2009b. Emerging biological functions of the vaccinia-related kinase (VRK) family. Histol Histopathol 24, 749-759.

Lancaster, O.M., Cullen, C.F., Ohkura, H., 2007. NHK-1 phosphorylates BAF to allow karyosome formation in the Drosophila oocyte nucleus. J Cell Biol 179, 817-824.

Molitor, T.P., Traktman, P., 2014. Depletion of the protein kinase VRK1 disrupts nuclear envelope morphology and leads to BAF retention on mitotic chromosomes. Mol Biol Cell 25, 891-903.

Newman, A.P., White, J.G., Sternberg, P.W., 1996. Morphogenesis of the C. elegans hermaphrodite uterus. Development 122, 3617-3626.

Oommen, K.S., Newman, A.P., 2007. Co-regulation by Notch and Fos is required for cell fate specification of intermediate precursors during C. elegans uterine development. Development 134, 3999-4009.

Pettitt, J., 2005. The cadherin superfamily. WormBook, 1-9.

Pettitt, J., Wood, W.B., Plasterk, R.H., 1996. cdh-3, a gene encoding a member of the cadherin superfamily, functions in epithelial cell morphogenesis in Caenorhabditis elegans. Development 122, 4149-4157.

Praitis, V., 2006. Creation of transgenic lines using microparticle bombardment methods. Methods Mol Biol 351, 93-107.

Reece-Hoyes, J.S., Shingles, J., Dupuy, D., Grove, C.A., Walhout, A.J., Vidal, M., Hope, I.A., 2007. Insight into transcription factor gene duplication from Caenorhabditis elegans Promoterome-driven expression patterns. BMC genomics 8, 27.

Riggi, N., Knoechel, B., Gillespie, S.M., Rheinbay, E., Boulay, G., Suva, M.L., Rossetti, N.E., Boonseng, W.E., Oksuz, O., Cook, E.B., Formey, A., Patel, A., Gymrek, M., Thapar, V., Deshpande, V., Ting, D.T., Hornicek, F.J., Nielsen, G.P., Stamenkovic, I., Aryee, M.J., Bernstein, B.E., Rivera, M.N., 2014. EWS-FLI1 utilizes divergent chromatin remodeling mechanisms to directly activate or repress enhancer elements in Ewing sarcoma. Cancer cell 26, 668-681.

Salzano, M., Vazquez-Cedeira, M., Sanz-Garcia, M., Valbuena, A., Blanco, S., Fernandez, I.F., Lazo, P.A., 2014. Vaccinia-related kinase 1 (VRK1) confers resistance to DNA-damaging agents in human breast cancer by affecting DNA damage response. Oncotarget 5, 1770-1778.

Schindler, A.J., Sherwood, D.R., 2011. The transcription factor HLH-2/E/Daughterless regulates anchor cell invasion across basement membrane in C. elegans. Dev Biol 357, 380-391.

Schober, C.S., Aydiner, F., Booth, C.J., Seli, E., Reinke, V., 2011. The kinase VRK1 is required for normal meiotic progression in mammalian oogenesis. Mech Dev 128, 178-190.

Sevilla, A., Santos, C.R., Barcia, R., Vega, F.M., Lazo, P.A., 2004a. c-Jun phosphorylation by the human vaccinia-related kinase 1 (VRK1) and its cooperation with the N-terminal kinase of c-Jun (JNK). Oncogene 23, 8950-8958.

Sevilla, A., Santos, C.R., Vega, F.M., Lazo, P.A., 2004b. Human vaccinia-related kinase 1 (VRK1) activates the ATF2 transcriptional activity by novel phosphorylation on Thr-73 and Ser-62 and cooperates with JNK. J Biol Chem 279, 27458-27465.

Sherwood, D.R., Butler, J.A., Kramer, J.M., Sternberg, P.W., 2005. FOS-1 promotes basement-membrane removal during anchor-cell invasion in C. elegans. Cell 121, 951-962.

Sherwood, D.R., Sternberg, P.W., 2003. Anchor cell invasion into the vulval epithelium in C. elegans. Dev Cell 5, 21-31.

Shirayama, M., Seth, M., Lee, H.C., Gu, W., Ishidate, T., Conte, D., Jr., Mello, C.C., 2012. piRNAs initiate an epigenetic memory of nonself RNA in the C. elegans germline. Cell 150, 65-77.

Tan, P.B., Lackner, M.R., Kim, S.K., 1998. MAP kinase signaling specificity mediated by the LIN-1 Ets/LIN-31 WH transcription factor complex during C. elegans vulval induction. Cell 93, 569-580.

Valbuena, A., Lopez-Sanchez, I., Lazo, P.A., 2008. Human VRK1 is an early response gene and its loss causes a block in cell cycle progression. PLoS ONE 3, e1642.

Vega, F.M., Sevilla, A., Lazo, P.A., 2004. p53 Stabilization and accumulation induced by human vaccinia-related kinase 1. Mol Cell Biol 24, 10366-10380.

Verghese, E., Schocken, J., Jacob, S., Wimer, A.M., Royce, R., Nesmith, J.E., Baer, G.M., Clever, S., McCain, E., Lakowski, B., Wightman, B., 2011. The tailless ortholog nhr-67 functions in the development of the C. elegans ventral uterus. Dev Biol 356, 516-528.

Waaijers, S., Boxem, M., 2014. Engineering the Caenorhabditis elegans genome with CRISPR/Cas9. Methods 68, 381-388.

Waters, K., Yang, A.Z., Reinke, V., 2010. Genome-wide analysis of germ cell proliferation in C.elegans identifies VRK-1 as a key regulator of CEP-1/p53. Dev Biol 344, 1011-1025.

Wiebe, M.S., Nichols, R.J., Molitor, T.P., Lindgren, J.K., Traktman, P., 2010. Mice deficient in the serine/threonine protein kinase VRK1 are infertile due to a progressive loss of spermatogonia. Biology of reproduction 82, 182-193.

Wiebe, M.S., Traktman, P., 2007. Poxviral B1 kinase overcomes barrier to autointegration factor, a host defense against virus replication. Cell host & microbe 1, 187-197.

Ziel, J.W., Hagedorn, E.J., Audhya, A., Sherwood, D.R., 2009. UNC-6 (netrin) orients the invasive membrane of the anchor cell in C. elegans. Nat Cell Biol 11, 183-189.

Figure Legends

Fig. 1. Schematic representation of uterine development. **(A)** The AC/VU decision. The two central cells of somatic gonad primordium, Z1.ppp and Z4.aaa, are specified as anchor cell (AC) and ventral uterine (VU) cell. Initially, both cells are equivalent and express LIN-12 (light blue) and its ligand LAG-2 (dark blue), however, stochastic differences in their expression are amplified by a positive feedback loop involving HLH-2. This leads eventually to a situation where one of the cells expresses exclusively LAG-2 and becomes the AC, whereas the other cells becomes a LIN-12-expressing VU cell. **(B)** The AC (dark blue) signals via LAG-2 and LIN-12 to six of twelve VU descendants to adopt a π cell fate. **(C-D)** The π cells divide once producing twelve π cells. During L4 larval stage the AC fuses with eight π cells to form the syncytial uterine seam cell (utse).

Fig. 2. Postembryonic expression of VRK-1. **(A)** Single-copy transgenic strain shows ubiquitous expression of VRK-1::mCherry. VRK-1 is expressed in neurons throughout the body, as well as in VPCs, AC (arrowhead), uterine tissue and germ line. Images were acquired using different microscope settings to compensate for

tissue-specific expression levels. Scale bar, 5μm. **(B)** Single-copy wild type *vrk-1* but not kinase-dead *vrk-1* K169E transgenes rescue *vrk-1(ok1181)* phenotypes. The number of fertile progeny and percentage of adults with Pvl are shown. Each circle represents the offspring from an individual founder (*n*=5-15 founders; 291-1335 progeny scored for Pvl phenotype). Horizontal black lines and colored error bars report the mean and standard error of the mean, respectively. (C) Kinase-dead VRK-1 K169E::mCherry is expressed and localized similarly to wild type VRK-1.

Fig. 3. VRK-1 acts independently from the HLH-2 pathway. **(A)** Expression of GFP::HLH-2 green in merge) in control animals and *vrk-1* mutants during P6.p 1-, 2-, 4-, and 6-8 cell stages. Scale bar, 5μm. **(B)** Quantification of GFP::HLH-2 intensity in the AC in control (dark grey) and *vrk-1* mutants (light grey). Average fluorescence intensity in *vrk-1* mutants was not significantly different from control animals. Error bars report the standard error of the mean.

Fig. 4. VRK-1 regulates anchor cell morphology. **(A)** Confocal images of control animals and *vrk-1* mutants showing AC expression of UNC-40::GFP, *PLC*δ^{PH}::mCherry**,** PAT-3::GFP and MIG-2::GFP at the P6.p 4-cell stage. Arrowheads indicate abnormal AC protrusions. Scale bar, 5μm. (**B)** Quantification of UNC-40, *PLC*δ^{PH}, PAT-3 and MIG-2 polarization in control (dark grey) and *vrk-1* mutants (light grey) at the P6.p 4-cell stage. Polarity in *vrk-1* mutants was not significantly different from control animals, except for PAT-3::GFP (p=0.004). Error bars report the standard error of the mean. (**C)** AC morphology is severely affected in *vrk-1* mutants (n=79) when compared with control animals (n=110), both in terms of cell body shape (upper graph) and presence of cell protrusions (lower graph) ($p<0.001$).

Fig. 5. The anchor cell does not fuse in *vrk-1* mutants. **(A)** Expression of *cdh-3*::GFP in control animals and *vrk-1* mutants. At the L3/L4 molt GFP is expressed in the AC and some of the VPCs in both genotypes. At the early L4 stage the AC fuses with uterine π cells to form the utse in control animals resulting in diffuse *cdh-3*::GFP localization. By contrast, expression of *cdh-3*::GFP is limited to the area of the AC in *vrk-1* mutants indicating lack of fusion. At mid L4 stage in *vrk-1* mutants GFP is still retained in the AC. Arrowheads denote the AC. Images were acquired using different microscope settings to optimize GFP visualization. Scale bar, 5μm. **(B)** VRK-

1::mCherry expression under control of the *fos-1c* promoter in uterine cells and AC rescues several *vrk-1* phenotypes, including the AC fusion in early L4, formation of the utse in mid L4 and a uterine lumen. Arrowheads indicate the AC, whereas arrows point to the utse. Scale bars, 5μm. **(C)** Quantification of AC fusion in control animals and *vrk-1* mutants. Lack of AC fusion was partially rescued by the uterine specific expression of VRK-1 under control of *fos-1c* promoter ($p<0.001$).

Fig. 6. VRK-1 is essential for proliferation and differentiation of uterine tissue. **(A)** Expression of NHR-67::GFP in the four pre-VU cells is not affected in *vrk-1* mutants at the L2 larval stage. **(B)** Lack of EGL-13::GFP expression demonstrates that uterine π cells are not properly specified in *vrk-1* mutants at the L4 larval stage. **(C)** Lack of VRK-1 expression causes severe defects in proliferation and nuclear morphology of the uterine cells in early L3 and L3/L4 animals. EMR-1::mCherry (red in merge) and HIS-72::GFP (green in merge) visualize nuclear envelopes and chromatin, respectively. White arrowheads denote examples of uterine cells, whereas arrows point to vulva cells. **(D)** *vrk-1* mutants at the early L3 larval stage have fewer and abnormally shaped nuclei expressing FOS-1A::YFP, indicative of defects in the proliferation and differentiation of uterine cells. **(E)** Uterine VRK-1::mCherry expression under control of the *fos-1c* promoter rescues the proliferation and differentiation defects as well as the Pvl phenotype. Scale bars, 5μm. **(F)** Expression of VRK-1::mCherry in uterine cells rescues *vrk-1* mutant phenotypes. The number of fertile progeny and percentage of adults with Pvl are shown. Each circle represents the progeny from a single founder (n=3-10). Horizontal black lines and colored error bars report the mean and standard error of the mean, respectively.

Fig. S1. (A) Postembryonic expression of VRK-1. Single-copy transgenic strains show ubiquitous expression of VRK-1::GFP and VRK-1::Dendra2. VRK-1 is expressed in hypodermal cells and neurons throughout the body, as well as in VPCs, AC (arrowheads), uterine tissue and germ line. Still images were acquired using different microscope settings to compensate for tissue-specific expression levels. Scale bar, 5μm. **(B)** VRK-1::GFP is much more abundant in transgenic strain YL255 generated by microparticle bombardment than in single-copy strain BN156 generated by MosSCI. Still images taken using identical microscope settings. Scale bar, 10μm.

Fig. S2. Expression of VRK-1 during vulval and uterine development. An *vrk-1* mutant L3 larva expressing VRK-1::mCherry was anaesthetized and observed by time-lapse confocal microscopy for a total a 6 hours. Series of 5 focal planes separated by 2 μm were acquired every 5 minutes and most relevant focal planes for each time point were manually selected to mount video 1. White arrowheads denote the AC, red arrowheads indicate VRK-1::mCherry accumulating at the nuclear envelope of cells entering mitosis and green arrowheads point to VRK-1::mCherry associated with chromatin during anaphase. Scale bar, 5μm.

Fig. S3. VRK-1 acts independently from the FOS-1 pathway. **(A)** Expression of FOS1A::YFP in control animals and *vrk-1* mutants during P6.p 1-, 2-, 4-, and 6-8 cell stages. Scale bar, 5μm. **(B)** Quantification of FOS-1A::YFP intensity in the AC at P6.p 1-, 2-, 4-, and 6-8 cell stages in control (dark grey) and *vrk-1* mutants (light grey). Average fluorescence intensity in *vrk-1* mutants was not significantly different from wild type animals. Error bars report the standard error of the mean.

Fig. S4. Uterine-specific expression of VRK-1 under control of the *fos-1c* promoter during early and mid- L4 larval stages. White arrowheads denote uterine cells expressing VRK-1::mCherry, whereas arrows indicate the VPCs, which do not expression VRK-1::mCherry. Note that much less VRK-1::mCherry is expressed from the *fos-1c* promoter, when compared with the *vrk-1* endogenous promoter (Fig. 2A), suggesting that even very low VRK-1 expression in the uterine tissue is sufficient to support uterine and vulval development. Images were acquired on a NIKON A1R confocal microscope with 561 nm laser power=40%; HV gain=200, while images in Fig. 2A were acquired using laser power=10-15% and HV gain=180. Scale bars, 5μm.

Fig. S5. Control animals and *vrk-1* mutants expressing GFP::HLH-2 in presumptive AC and VU cells at the L2 larval stage were observed by confocal microscopy **(A)**. **(B)** The ratio between the average fluorescence intensity in the presumptive AC vs VU cells in *vrk-1* mutants was not significantly different from wild type animals. Scale bars, 5μm. Error bars report the standard error of the mean.

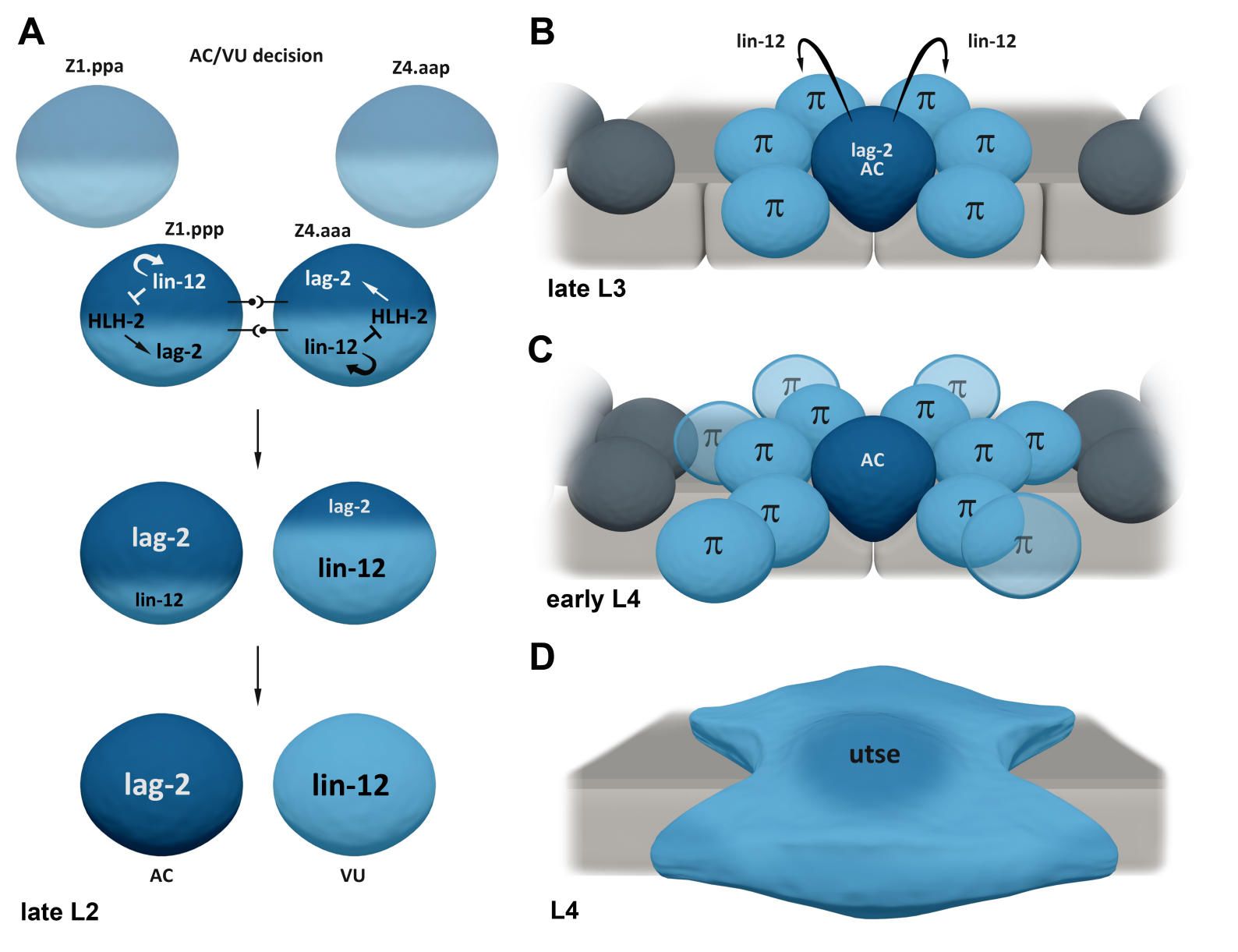
A
AC/VU decision
Z1.ppa
Z4.aap
Z1.ppp
Z4.aaa
lin-12
HLH-2
lag-2
lag-2
HLH-2
lin-12
lag-2
lin-12
lag-2
lin-12
lag-2
lin-12
AC
VU
late L2
B
lin-12
lin-12
lag-2
AC
late L3
C
AC
early L4
D
utse
L4

Figure 2

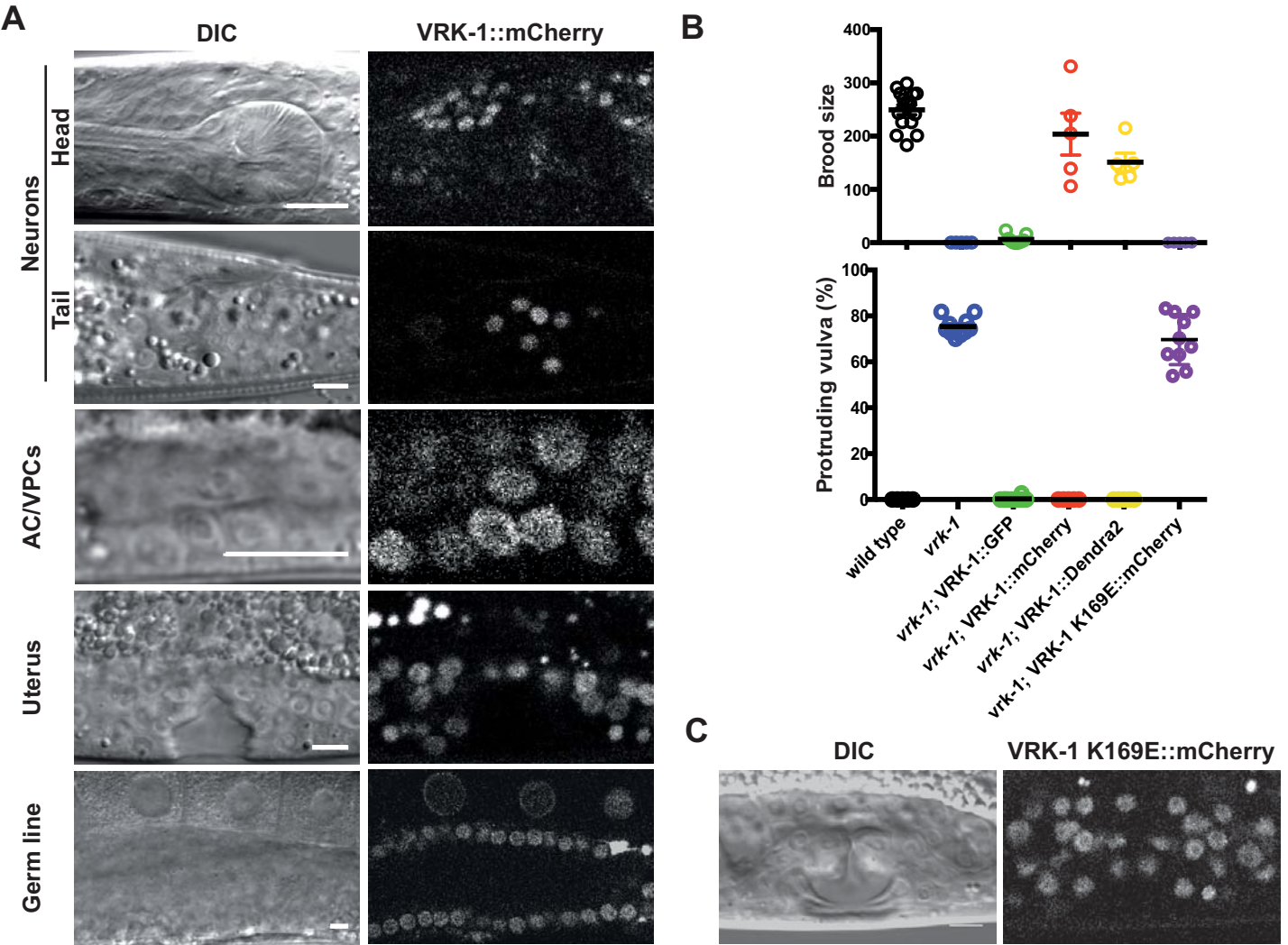
A
DIC
VRK-1::mCherry
Neurons
Head
Tail
AC/VPCs
Uterus
Germ line
B
Brood size
400
300
200
100
0
Protruding vulva (%)
100
80
60
40
20
0
wild type
vrk-1
vrk-1; VRK-1::GFP
vrk-1; VRK-1::mCherry
vrk-1; VRK-1::Dendra2
vrk-1; VRK-1 K169E::mCherry
C
DIC
VRK-1 K169E::mCherry

Figure 3

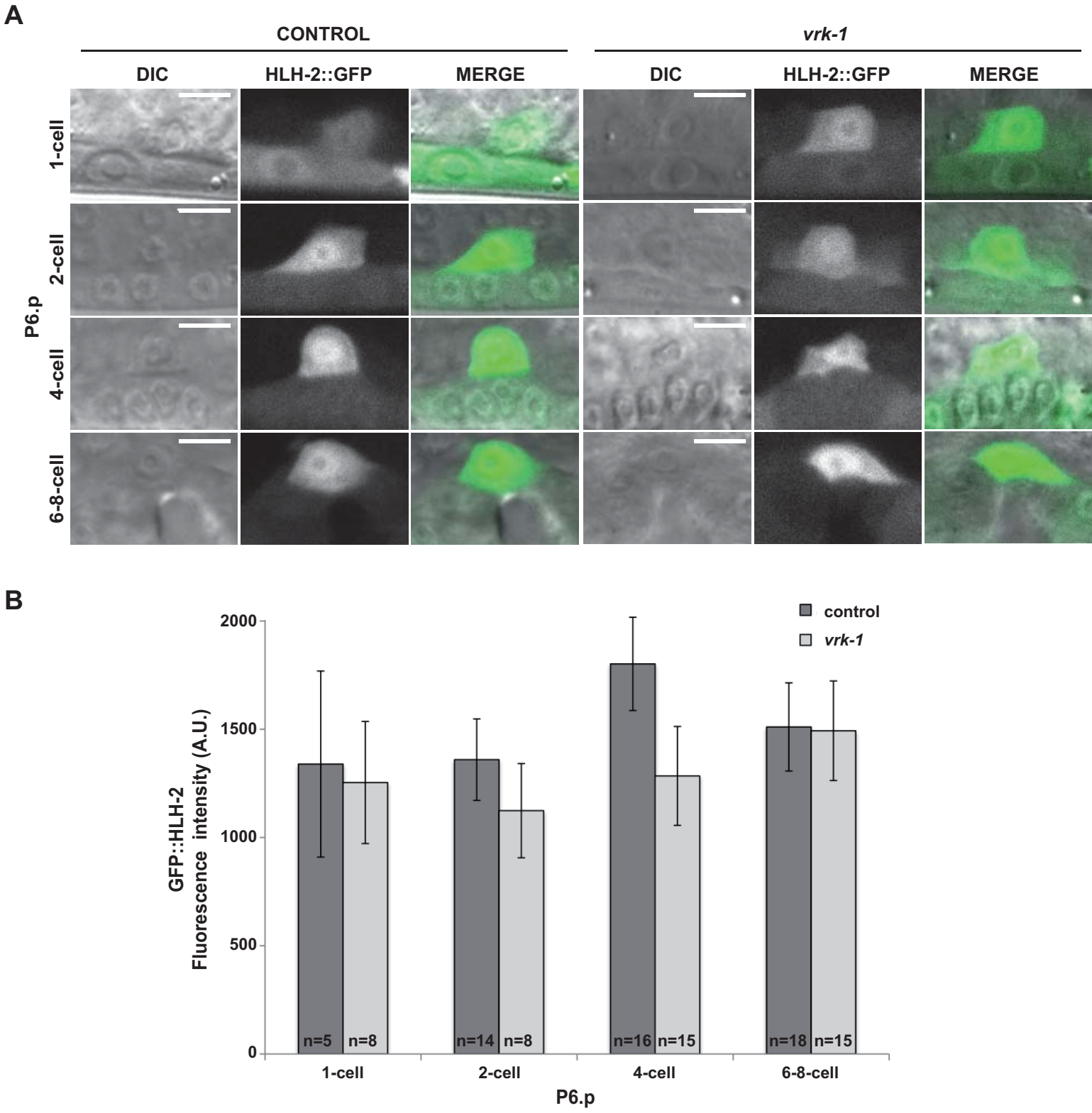
A
CONTROL
vrk-1
DIC
HLH-2::GFP
MERGE
DIC
HLH-2::GFP
MERGE
P6.p
1-cell
2-cell
4-cell
6-8-cell
B
control
vrk-1
GFP::HLH-2
Fluorescence intensity (A.U.)
2000
1500
1000
500
0
n=5
n=8
n=14
n=8
n=16
n=15
n=18
n=15
1-cell
2-cell
4-cell
6-8-cell
P6.p

Figure 4

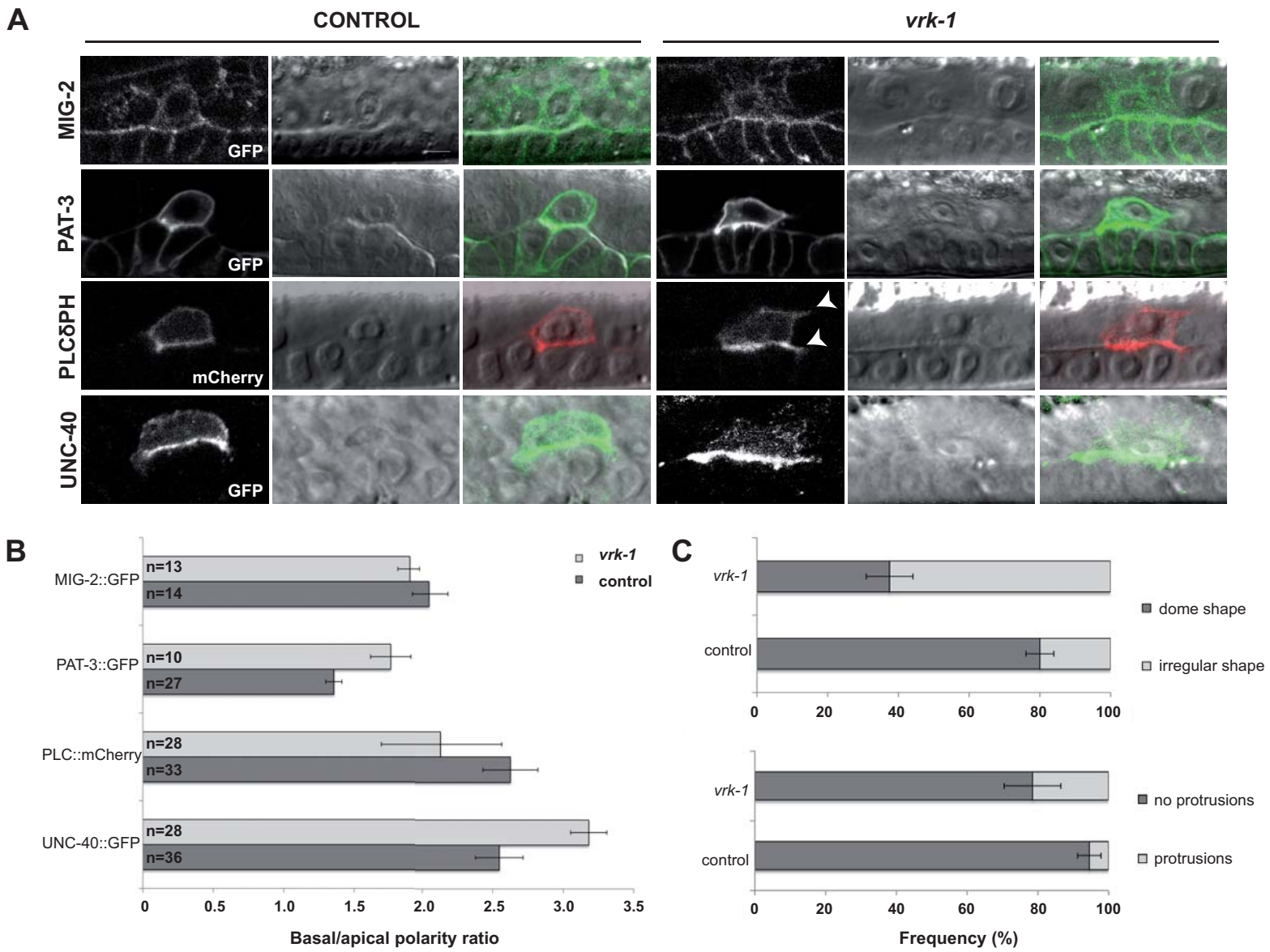
A
CONTROL
vrk-1
MIG-2
PAT-3
PLCδPH
UNC-40
GFP
mCherry
B
vrk-1
control
MIG-2::GFP
n=13
n=14
PAT-3::GFP
n=10
n=27
PLC::mCherry
n=28
n=33
UNC-40::GFP
n=28
n=36
0
0.5
1.0
1.5
2.0
2.5
3.0
3.5
Basal/apical polarity ratio
C
vrk-1
control
dome shape
irregular shape
0
20
40
60
80
100
vrk-1
control
no protrusions
protrusions
0
20
40
60
80
100
Frequency (%)

Figure 5

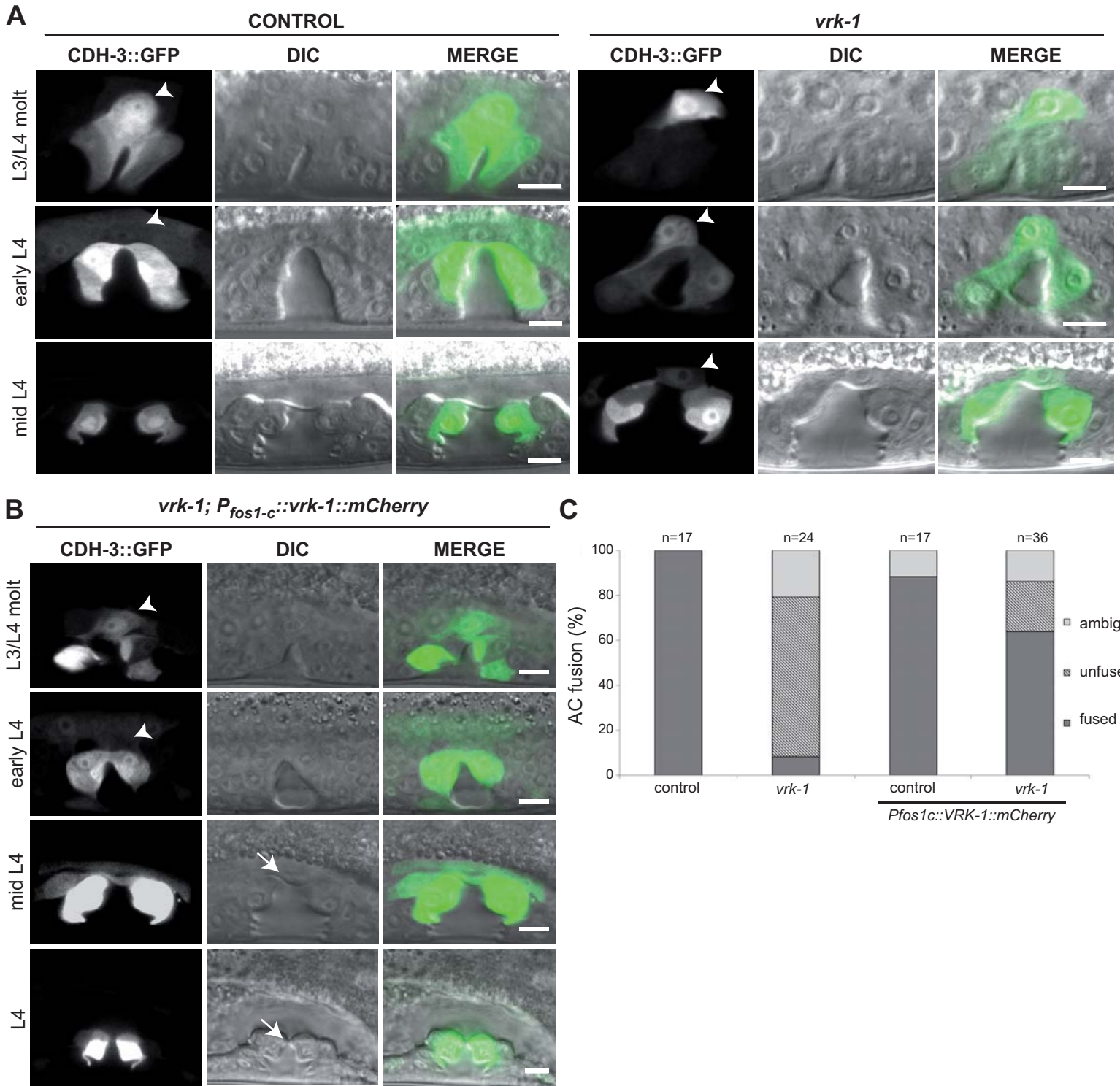
A
CONTROL
vrk-1
CDH-3::GFP
DIC
MERGE
CDH-3::GFP
DIC
MERGE
L3/L4 molt
early L4
mid L4
B
vrk-1; Pfos1-c::vrk-1::mCherry
CDH-3::GFP
DIC
MERGE
L3/L4 molt
early L4
mid L4
L4
C
AC fusion (%)
100
80
60
40
20
0
n=17
n=24
n=17
n=36
ambiguous
unfused
fused
control
vrk-1
control
vrk-1
Pfos1c::VRK-1::mCherry

Figure 6

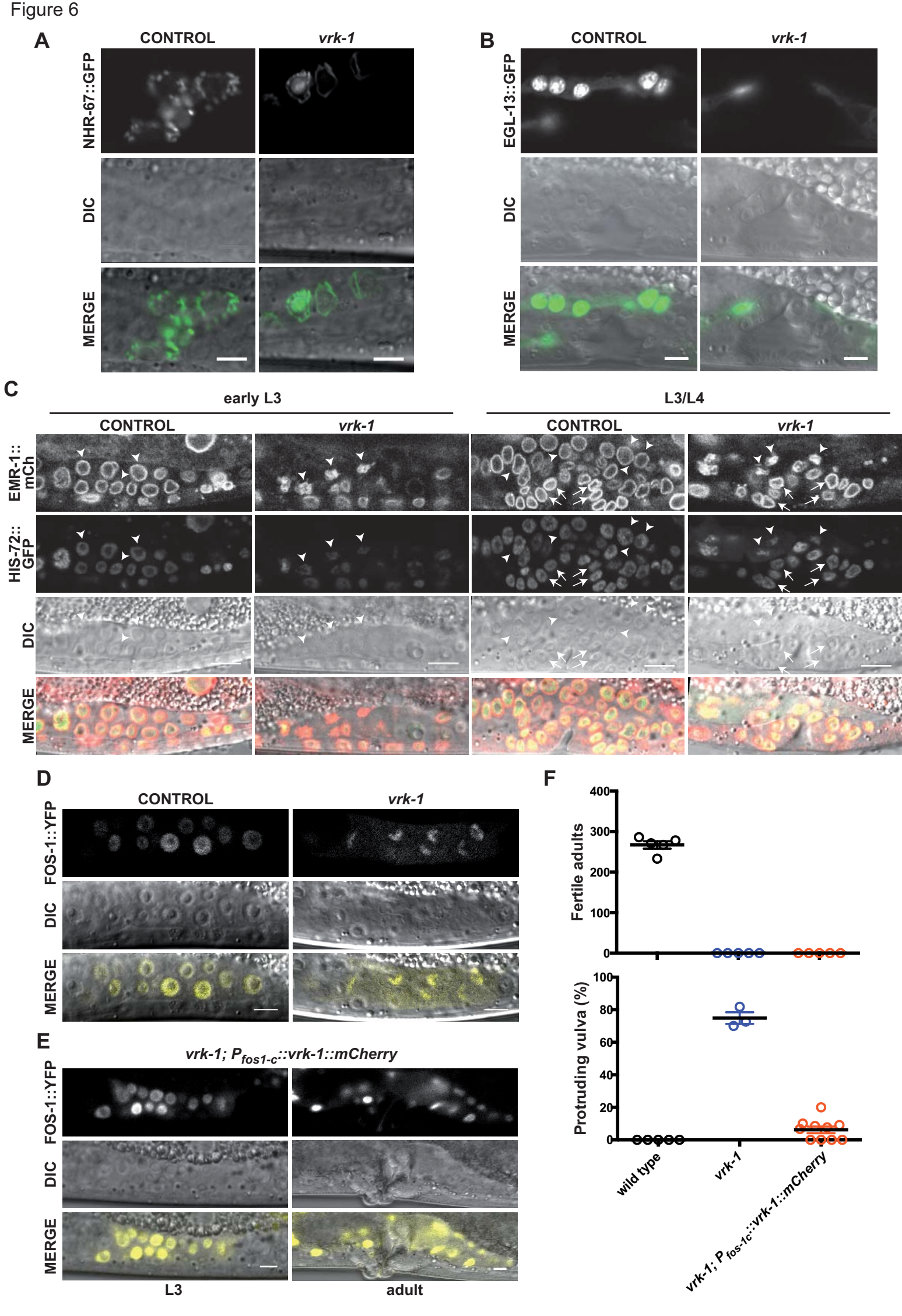
A
CONTROL
vrk-1
NHR-67::GFP
DIC
MERGE
B
CONTROL
vrk-1
EGL-13::GFP
DIC
MERGE
C
early L3
L3/L4
CONTROL
vrk-1
CONTROL
vrk-1
EMR-1::mCh
HIS-72::GFP
DIC
MERGE
D
CONTROL
vrk-1
FOS-1::YFP
DIC
MERGE
E
vrk-1; Pfos1-c::vrk-1::mCherry
FOS-1::YFP
DIC
MERGE
L3
adult
F
Fertile adults
400
300
200
100
0
Protruding vulva (%)
100
80
60
40
20
0
wild type
vrk-1
vrk-1; Pfos1c::vrk-1::mCherry

Supplementary Figure S1

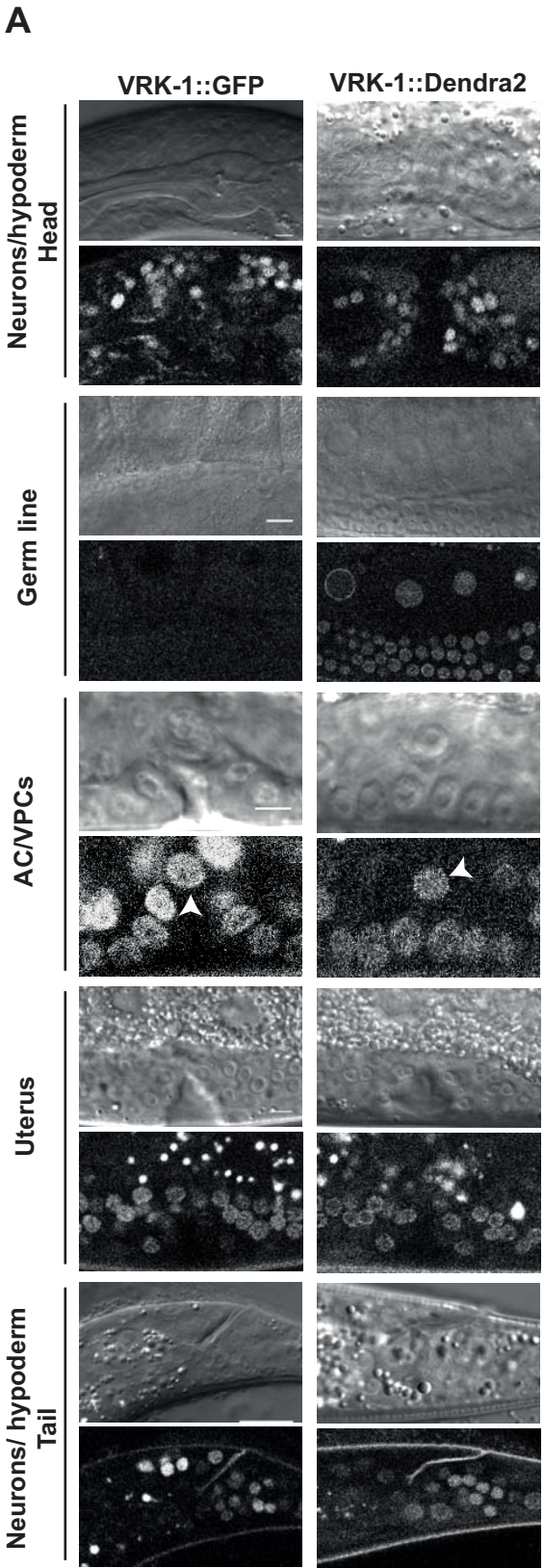

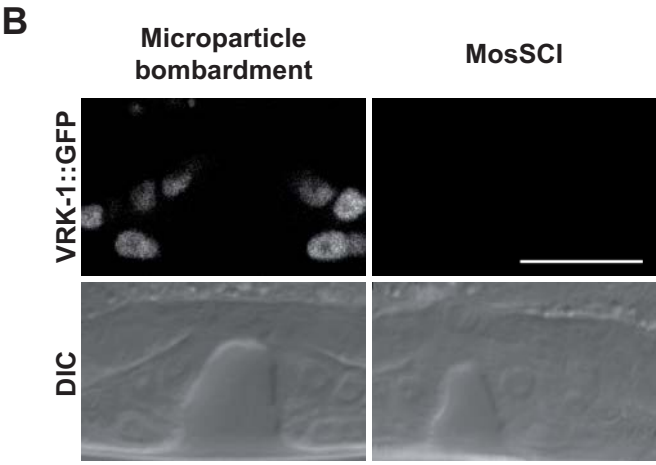

Supplementary Figure S2

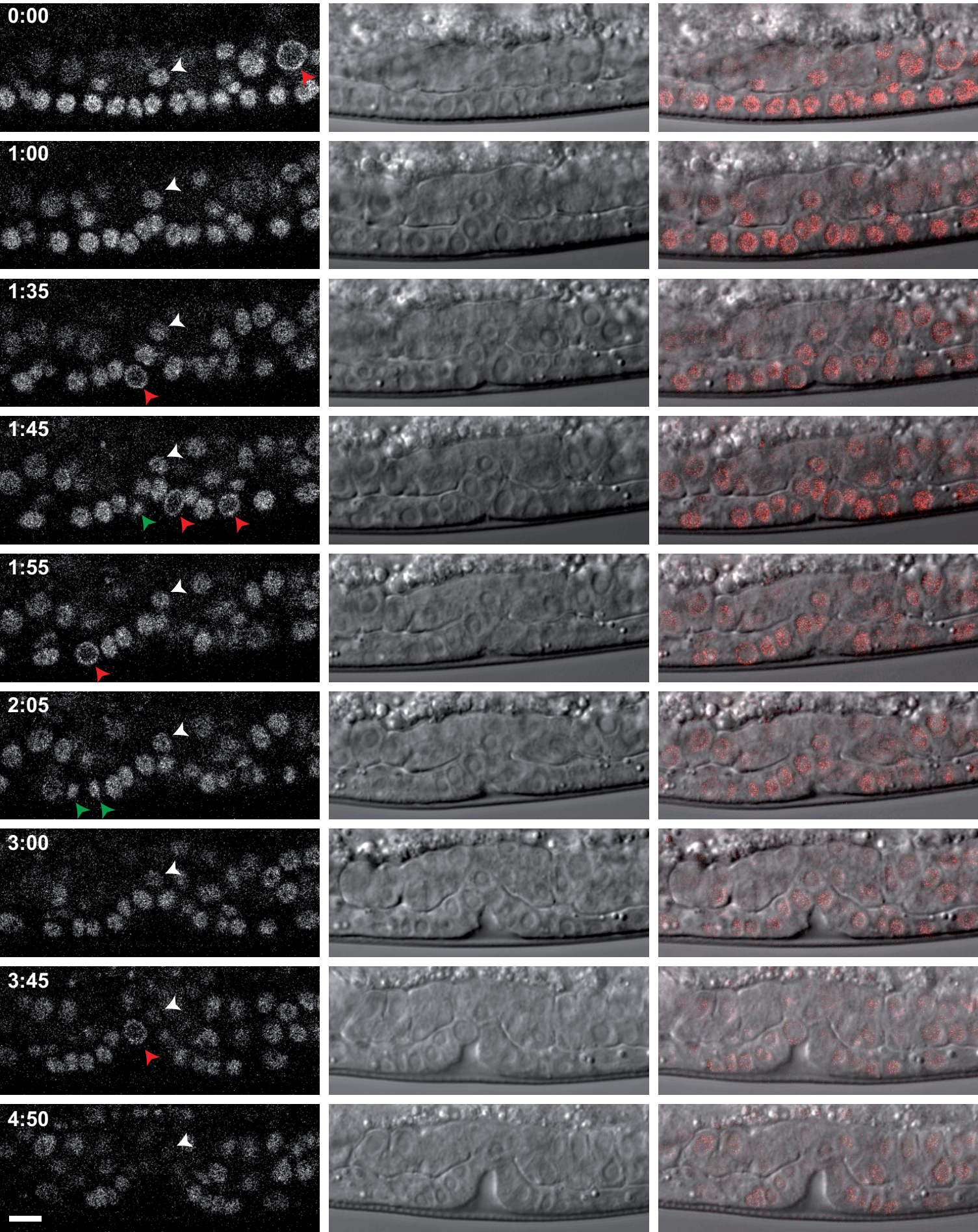

Supplementary Figure S3

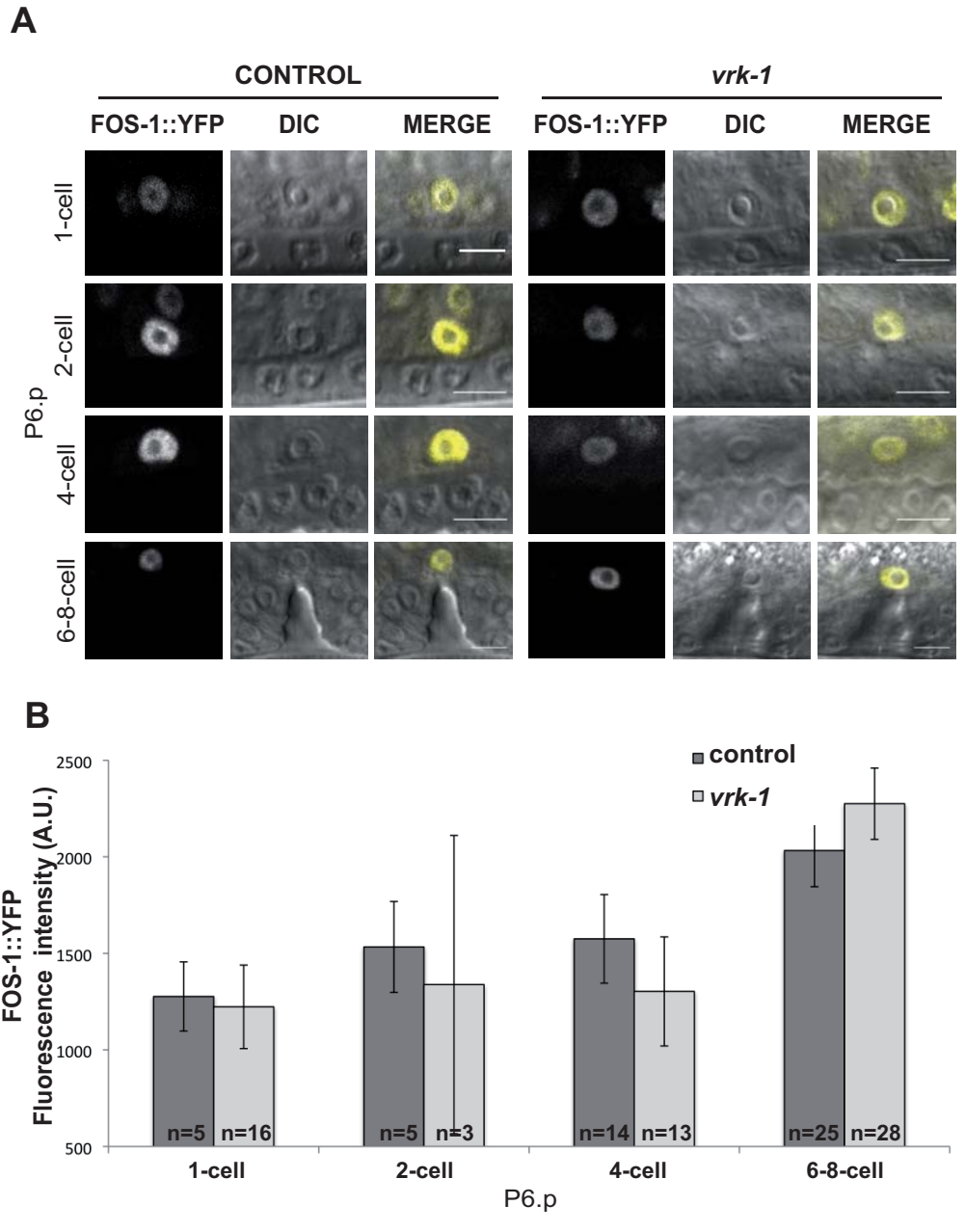

Supplementary Figure S4